Ab Initio Study of Peroxyacetic Nitric Anhydride and Peroxyacetyl Radical: Characteristic Infrared Band of Peroxyacetyl Radical

Byung Jin Mhin* and Won Young Chang

Department of Chemistry, PaiChai University, 439-6 Doma-dong, Seoku, Taejun 302-735, Korea

Jin Yong Lee and Kwang S. Kim

National Creative Research Initiative Center for Superfunctional Materials and Department of Chemistry, Pohang University of Science and Technology, San 31, Hyojadong, Namgu, Pohang 790-784, Korea

Received: September 22, 1999; In Final Form: December 16, 1999

The equilibrium geometries, the bond dissociation energies, harmonic vibrational frequencies, and infrared intensities of peroxyacetic nitric anhydride (PAN), peroxyacetyl radical (PA), and NO_2 which are important species in environmental chemistry, have been studied using high level of ab initio calculations. The global minimum energy conformation of the PAN molecule is found to be *s-cis*-PAN. The predicted enthalpy and entropy changes at 1 atm and 298.15 K for the thermal decomposition of PAN are 25.8 kcal/mol and 42.3 cal/(mol·K), respectively. These values are in excellent agreement with the experimental values. A characteristic IR band of PAN appears at 1232 cm^{-1}, which is a CH_3 rocking mode coupled with CO and OO stretches. The corresponding band of the PA radical appears at 1216 cm^{-1}, about 10 cm^{-1} lower than that of PAN. Thus, determining the concentrations of PAN based on only this band would not be so reliable. We find that the PA radical has a strong IR band at 1150 cm^{-1} due to the O−O stretch mode, while the PAN molecule has the corresponding band at 977 cm^{-1}. Since PAN and the PA radical do not have other IR bands at this region, this characteristic band could be used for identification and measurement of the PA radical and thus for spectroscopic study of thermal decomposition mechanism of PAN.

1. Introduction

Reactive odd-nitrogen compounds, abbreviated NO_y, play an important role in the chemistry of the lower atmosphere.[1,2] NO_y has traditionally been defined as the sum of simple nitrogen oxides ($NO + NO_2$) and atmospheric products of NO_x including all the intermediate oxidation states. It is involved in the production of acidic rain and ozone, since these intermediate oxidation state species serve as reservoirs for the storage and transport of NO_x to the regional and global atmosphere. Among the intermediate ones, peroxyacetic nitric anhydride (PAN, often called peroxyacetyl nitrate) is one of the most important organic species in the atmosphere due to its high stability compared with other acyl peroxynitrates. This molecule was discovered by IR measurement of photochemical smog in the late 1950s[3] and has been considered an important component of photochemical smog ever since.[4] Subsequent studies have shown that not only PAN is found in NO_x-rich urban environments, but also it is one of the most abundant reactive nitrogen-containing species in the clean troposphere.[5] PAN forms in urban areas where the photochemistry of nonmethane hydrocarbons coincides with high NO_x concentrations and exists in rapid equilibrium with its radical precursors (PA radicals). PAN is transported by convection into the upper troposphere where it may travel hundreds of kilometers before descending in a remote location. Since PAN is a temporary NO_x reservoir, the net result of this long-range transportation is to distribute NO_x from polluted urban environments into pristine environments where normal NO_x concentrations are otherwise negligible.

* To whom correspondence should be addressed. Fax: +82−42−520−5375. Phone: +82-42-520-5611. E-mail: mhin@woonam.paichai.ac.kr.

PAN is generated by the reaction of peroxyacetyl (PA) radical with nitrogen dioxide[6] and is removed from the atmosphere by the reaction with OH, photolysis, thermal decomposition, and deposition.[1]

$$CH_3C(O)OO + NO_2 + M \rightarrow CH_3C(O)OONO_2 + M \quad (1)$$

$$CH_3C(O)OONO_2 \rightarrow CH_3C(O)OO + NO_2 \quad (2)$$

The dominant atmospheric removal mechanism of PAN is the thermal decomposition and photolysis, which depends on the altitude. Thermal decomposition is dominant in the lower atmosphere (<7 km), while photolysis domonates in the upper troposphere. The reaction of PAN with OH radical is not competitive with these processes in any region of the atmosphere. Hence, most studies of PAN in the atmosphere have shown that its lifetime in the troposphere is closely related to the thermal decomposition process,[4a] and the important role of PAN depends on the equilibrium constant for the reactions.[1,2] A recent theoretical study on the unimolecular dissociation pathways of PAN gave an implication for the atmospheric decomposition of PAN.[7]

Spectroscopic methods have been particularly important in the study of organic nitrate chemistry. Infrared absorption spectroscopy has proved to be a powerful technique for structural determination and is used for gas-phase mechanistic studies. Thus, the temperature dependence of this reaction has been studied by several groups,[8−13] especially with IR spectroscopy. The experimental spectroscopy studies[14−17] have shown that PAN has two characteristic IR bands at about 795 and 1165 cm^{-1}. The former is a characteristic frequency of all peroxy

10.1021/jp993396d CCC: $19.00
Published on Web 02/24/2000

nitrates, which has inconsistent assignment as the O−N stretching or NO_2 scissoring modes, and the latter is a feature of PAN. Thus, most of the mechanism studies of thermal decomposition of PAN have been done with the IR absorption band at 1165 cm^{-1}, which was assigned to C−O stretching. Our normal-mode analysis shows that IR bands at 795 and 1165 cm^{-1} are assigned as the NO_2 scissoring and CH_3 rocking modes, respectively.

The determination of vibrational spectra and thermodynamic quantities by ab initio computational methods has been exploited to identify unknown structures of experimentally observed molecular species and clusters.[18] There is no experimental structural information on PAN and the PA radical, while the thermodynamic quantities for reaction 2 were determined experimentally.[19] The fundamental vibrational frequencies of PAN are also available from experiments.[11]

Jursic[20] has computed the structures and energies of PAN using density functional theory and compared the stability of the conformation on the basis of the binding energy (D_e). To determine the conformation of the PAN compound based on the experimental data (thermodynamic quantities and vibrational frequencies), we investigated structures, energetics, and spectra for PAN, NO_2, and the PA radical. Presented here is a comparison of the calculated vibrational spectra with the normal-mode analysis including potential energy distribution with experiments. The present study is the first theoretical attempt to characterize the vibrational spectra of PAN and the PA radical.

2. Computational Methods

To investigate the structural properties and normal vibrational modes, we have carried out ab initio calculations at the levels of hybrid Becke-3−Lee−Yang−Parr parameters (B3LYP) density functional theory (DFT), Moller−Plesset second-order perturbation theory (MP2), and coupled clusters method with single, double, and noniterative triple excitations [CCSD(T)]. The geometry optimizations were done at the above levels of theory, and the optimized geometries were characterized as local minima by harmonic vibrational frequency analysis. All the calculations were carried out with 6-31G(d) basis sets using a Gaussian 94 suite of programs.[21] The bond dissociation energies (D_e) were given with respect to the sum of the ground-state total energies of the dissociation products. The predicted D_e showed large discrepancies depending on the levels of theory. To evaluate the D_e more accurately, we performed higher levels of calculation (MP3, MP4SDQ, CCSD, CCSD(T)) at the MP2/6-31G(d) optimized geometries, where CC represents the coupled cluster method, and S, D, and (T) denote single, double, and noniterative triple excitations, respectively. The thermodynamic quantities and the zero-point vibrational energies were obtained from the harmonic vibrational frequencies by the standard statistical mechanical calculations with rigid rotor and harmonic oscillator approximations.[22]

Generally, ab initio harmonic vibrational frequencies are overestimated.[23] Since this overestimation is found to be consistent, the constant[23] or exponential[24] scaling method is often employed. Constant scale factors suitable for MP2/6-31G(d)-predicted frequencies are between 0.921 and 0.96. Rauhut and Pulay[25] developed a scaling factor (0.963) for the B3-LYP/6-31G(d) method. We choose the internal coordinates, as shown in Figure 1, in accordance with Pulay's recommendation.[26] The normal vibrational modes were analyzed with these internal coordinates, and the assignment of the normal modes was based on potential energy distribution (PED) obtained from normal-mode analysis.

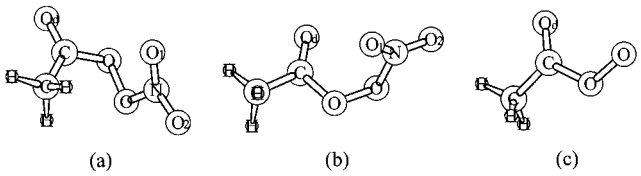

(a) (b) (c)

Figure 1. Structures of *s-trans*-PAN (a), *s-cis*-PAN (b), and PA (c).

TABLE 1: Structural Parameters for *s-cis*-PAN, *s-trans*-PAN, and PA + NO_2[a]

	s-cis-PAN		s-trans-PAN		PA + NO_2		
	B3LYP	MP2	B3LYP	MP2	B3LYP	MP2	CCSD(T)
r_{O-O}	1.4096	1.4258	1.4167	1.4265	1.3277	1.3328	1.3495
r_{O-N}	1.5074	1.5471	1.5150	1.5647			
r_{N-O1}	1.1964	1.2034	1.1963	1.2031	1.2026	1.2164	1.2150
r_{N-O2}	1.1971	1.2066	1.1974	1.2063	1.2026	1.2164	1.2150
r_{C-O}	1.5064	1.4999	1.5037	1.4989	1.5020	1.4964	1.5023
$r_{C=Od}$	1.1952	1.2060	1.1966	1.2073	1.1901	1.1991	1.1988
r_{C-C}	1.5064	1.4999	1.5037	1.4989	1.5020	1.4964	1.5023
$\angle CCO_d$	128.8	128.8	127.6	127.3	129.8	129.9	129.6
$\angle CCO$	107.6	107.4	117.8	117.6	107.7	107.2	107.6
$\angle OCO_d$	123.6	123.8	114.6	115.0	122.5	122.9	122.8
$\angle O_1NO_2$	133.6	135.1	133.8	135.5	134.0	133.8	133.8
$\angle O_1NO$	109.4	108.7	109.6	108.8			
$\angle O_2NO$	116.9	116.2	116.6	115.6			
$\angle COO$	111.2	110.2	113.5	112.4	113.0	111.9	111.9
$\angle OON$	109.1	107.3	108.9	106.7			
$\tau[O_dCOO]$	−3.1	−4.7	−177.0	−178.4	0.0	0.0	0.0
$\tau[COON]$	85.1	80.7	−97.0	−94.7			
$\tau[OONO_1]$	−2.6	−0.6	10.7	10.5			

[a] Bond lengths are in angstroms, and angles and dihedral angles are in degrees. See Figure 1 for the definition of structural parameters for bond lengths and bond angles. The values of $\tau[O_dCOO]$, $\tau[COON]$, and $\tau[OONO_1]$ are dihedral angles about C−O, O−O, and O−N bonds, respectively.

3. Results and Discussion

The geometrical parameters for *s-cis*-PAN, *s-trans*-PAN, PA, and NO_2 are listed in Table 1. There is no experimental data for the structures of PAN and the PA radical. For PA, we used CCSD(T) geometry optimization and find that the O−O bond length (r_{O-O}), C−O bond length (r_{C-O}), and C−C bond length (r_{C-C}) increase compared with the MP2 results, while the C═O bond length ($r_{C=Od}$) decreases. The PAN compound has four single bonds (CC, CO, OO, and ON); hence there are many possible rotational isomers. Among them, we studied two rotational isomers of PAN about the CO single bond (*s-cis*-PAN and *s-trans*-PAN). The dihedral angles ($\tau[O_dCOO]$) about the C−O bond of these two isomers are −4.7° and −178.4° for *s-cis*-PAN and *s-trans*-PAN, respectively. The dihedral angles ($\tau[COON]$) about the O−O bond are 80.7° (85.1°) and −94.7° (−97.0°) for the *s-cis*-PAN and the *s-trans*-PAN, respectively.

The MP2-predicted bond lengths tend to be longer than B3LYP-predicted ones except for the CC single bond length (r_{C-C}). The MP2-predicted structures for both *s-cis*-PAN and *s-trans*-PAN are almost the same as B3LYP-predicted ones, and the bond length difference for these two conformers is small (Table 1). The noticeable differences in bond lengths for *s-cis*-PAN, *s-trans*-PAN, and PA are shown in r_{O-O} and r_{O-N}. The values of r_{O-O} and r_{O-N} for *s-cis*-PAN are shorter than those for *s-trans*-PAN. The bond angles of $\angle OCC$ and $\angle OCO_d$ are quite different in *s-cis*-PAN and *s-trans*-PAN. The values of $\angle OCC$ and $\angle OCO_d$ for *s-cis*-PAN are 107.6° and 123.6°, respectively, while those for *s-trans*-PAN are 117.8° and 114.6°, and those for the PA radical are 107.7° and 122.5°. The bond

TABLE 2: Bond Dissociation Energies and Thermodynamic Quantities for *s-cis*-PAN → PA + NO_2 and *s-trans*-PAN → PA + NO_2 at 298.15 K and 1 atm[a]

	s-cis-PAN → PA + NO_2				s-trans-PAN → PA + NO_2		
	exp[b]	B3LYP	MP2	CCSD(T)[c]	B3LYP	MP2	CCSD(T)[c]
$\Delta E_e(D_e)$		27.5	37.2	27.5	24.5	33.3	23.9
$\Delta E_o(D_o)$		24.0	34.7	25.1	21.0	30.9	21.4
ΔE		24.3	34.9	25.2	21.4	31.1	21.7
ΔH	26 ± 2	24.9	35.5	25.8	22.0	31.7	22.2
ΔG		12.1	22.9	13.2	8.6	18.6	9.1
ΔS	42 ± 2	42.7	42.3	42.3	44.8	44.1	44.1

[a] D_e, D_o, ΔE, ΔH, and ΔG are in kcal/mol, and ΔS is in cal/(mol·K). [b] Reference 19. [c] CCSD(T) calculations were carried out at the MP2 optimized geometries.

angles of *s-cis*-PAN are similar to those of the PA radical. The other bond angles are similar.

Bond dissociation energies and thermodynamic quantities are listed in Table 2. We discuss the energetics on the basis of the results of CCSD(T) if otherwise specified. The *s-cis*-PAN is more stable than *s-trans*-PAN by 3.64 kcal/mol. The population of *s-trans*-PAN would be negligible at 298.15 K. In this paper PAN represents the *s-cis*-PAN. The enthalpy and entropy changes for the reaction 2 were experimentally determined to be about 26 ± 2 kcal/mol and 42 ± 2 cal/(mol·K) at 1 atm and 298.15 K, respectively.[19] However, at the UHF level, the cleavage of the O−N bond of the PAN molecule was predicted to be exothermic; therefore, an electron correlation was necessary in this study. For MP2 results, the PAN molecule is stabilized, and the reaction is correctly predicted as endothermic. However, the MP2-predicted D_o (34.7 kcal/mol) is much larger than the experimental enthalpy change (26 kcal/mol). The MP2 calculations seem to overestimate the "true" magnitude of the electron correlation effect. In previous theoretical work[20,27] on bond breaking or formation, it is reported that ab initio calculations may not produce satisfactory results even at the MP2 level. The CCSD(T)//MP2 results showed that the MP2 calculations overestimated the electron correlation. The CCSD(T)-predicted D_o is 25.1 kcal/mol, which is in excellent agreement with experiment. The B3LYP-predicted D_o (24.1 kcal/mol) is very close to this value. The CCSD(T)/DFT-predicted enthalpy and entropy changes at 1 atm and 298.15 K are 25.8/24.9 kcal/mol and 42.3/42.7 cal/(mol·K), respectively. These values are in good agreement with the experimental values. But, for *s-trans*-PAN, the CCSD(T)/DFT-predicted enthalpy and entropy changes at 1 atm and 298.15 K are 22.2/22.0 kcal/mol and 44.1/44.8 cal/(mol·K), respectively. This supports that *s-cis*-PAN should be the experimentally observed structure for PAN.

Spectroscopic methods have been exploited in the research field of atmospheric chemistry, especially in organic nitrate chemistry. Infrared absorption spectroscopy has been proved to be a powerful technique for structural determination and has been used for gas phase mechanistic study. The PAN compound was originally identified by long-path IR spectroscopy,[3,4b] and most studies on the thermal decomposition mechanism of PAN have been done by the use of IR spectroscopy. Table 3 lists the MP2- and B3LYP-predicted harmonic vibrational frequencies and their IR intensities. The B3LYP-predicted IR spectra for PAN and PA + NO_2 are shown in Figure 2. This provides a reference for the chemical characterization or measurement of

TABLE 3: Predicted Harmonic Vibrational Frequencies and Their IR Intensities (in Parentheses) for PANs, PA, and NO_2[a]

	s-cis-PAN				s-trans-PAN		PA + NO_2	
	expt[b]	ref 15	DFT	MP2	DFT	MP2	DFT	MP2
CH_3 str	3013	3020 (27)	3186 (1.8)	3251 (0.7)	3188 (2.2)	3252 (1.0)	3188 (2.5)	3255 (1.0)
CH_3 str	2950		3144 (1.7)	3219 (0.4)	3148 (1.4)	3225 (1.0)	3135 (1.4)	3216 (0.2)
CH_3 str	2950		3076 (0.1)	3130 (0.0)	3080 (0.5)	3135 (0.5)	3073 (0.1)	3129 (0.1)
C═O str	1720	1841 (322)	1909 (194)	1890 (157)	1907 (237)	1978 (165)	1929 (194)	1921 (155)
NO_2 asym str	1737	1741 (808)	1847 (348)	1978 (179)	1844 (354)	1879 (205)	1727 (324)	2299 (2114)
CH_3 asym def	1478	1430 (27)	1501 (11)	1534 (13)	1509 (12)	1543 (12)	1497 (10)	1532 (14)
CH_3 asym def	1428	1372 (48)	1498 (12)	1533 (12)	1495 (6.1)	1529 (7.5)	1495 (13)	1532 (11)
CH_3 sym def	1418		1422 (28)	1454 (37)	1423 (33)	1455 (39)	1424 (29)	1457 (36)
NO_2 sym str	1397	1302 (405)	1373 (231)	1335 (164)	1373 (221)	1333 (148)	1407 (0.6)	1384 (0.1)
CH_3 rocking	1092	1163 (477)	1193 (249)	1232 (245)	1210 (284)	1249 (284)	1182 (61)	1216 (87)
CH_3 rocking′	1087	1055 (25)	1077 (7.7)	1097 (6.6)	1073 (7.1)	1090 (6.0)	1062 (9.2)	1088 (8.2)
CH_3 rocking	1040	990 (35)	1007 (30)	1028 (27)	1023 (24)	1044 (22)	1001 (24)	1026 (24)
OO str	1286	9291 (61)	977 (35)	937 (44)	946 (63)	933 (64)	1143 (124)	1150 (184)
CO str			841 (51)	853 (46)	805 (43)	817 (26)	750 (72)	780 (93)
NO_2 bending	744	7931 (247)	807 (190)	768 (176)	792 (151)	760 (166)	749 (8.0)	753 (7.3)
CC str	884	822 (22)	727 (1.6)	721 (10)	728 (23)	700 (22)	653 (32)	665 (28)
NO_2 wagging	645	718 (17)	724 (11)	697 (7.1)	688 (9.7)	672 (15)		
			610 (38)	596 (19)	560 (17)	564 (10)		
			580 (12)	575 (45)	553 (21)	510 (49)	544 (5.2)	553 (5.3)
NO str + CCO + CCO_d	904	574	493 (8.7)	450 (45)	502 (14)	505 (18)		
			371 (3.7)	361 (23)	409 (9.9)	367 (58)		
			332 (3.2)	325 (11)	329 (1.8)	329 (9.0)	414 (1.5)	422 (1.3)
			315 (2.0)	319 (1.8)	318 (5.7)	324 (8.0)	303 (1.6)	311 (1.6)
τ[COON] + τ[$OONO_1$]	82		98 (0.5)	116 (0.3)	178 (0.3)	200 (0.2)		
τ[HCCO] + τ[O_dCOO]	62		94 (1.4)	100 (2.0)	93 (1.2)	94 (0.4)	136 (0.2)	143 (0.4)
τ[COON] + τ[$OONO_1$]	55		81 (1.6)	80 (1.0)	83 (1.3)	82 (0.4)		
τ[HCCO] + τ[O_dCOO]	49		44 (0.8)	46 (1.4)	72 (1.6)	77 (1.7)	69 (0.4)	88 (0.3)

[a] $\tau 1$, $\tau 2$, $\tau 3$, and $\tau 4$ represent the dihedral angles about C−C, C−O, O−O, and O−N bonds, respectively. Frequencies are in cm^{-1}, and IR intensities are in km/mol. [b] Reference 11.

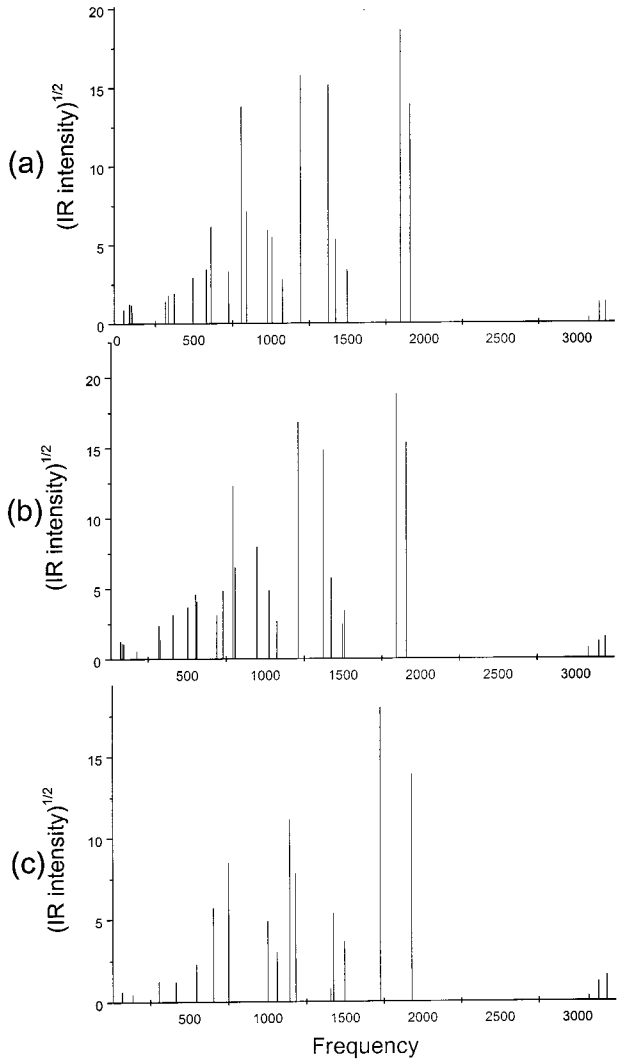

Figure 2. IR spectra for (a) *s-cis*-PAN, (b) *s-trans*-PAN, and (c) PA+NO_2.

these compounds. The MP2-predicted vibrational frequencies are larger than DFT-predicted ones for stretching and bending modes, as expected from the scaling factors. Furthermore, the MP2/6-31G(d)-predicted frequencies for NO_2 and the nitroperoxy group ($-O-O-NO_2$) were seriously deviated, as previously reported.[23] But, the bending and torsional modes show the opposite behavior.

As shown in Figure 2, the vibrational frequencies of PAN and PA+ NO_2 are quite different. It should be noted that the O−O stretching frequency is drastically shifted from 980 cm^{-1} at PAN to 1150 cm^{-1} at PA. Furthermore, since there are no other interfering IR active bands in this region, this band can be used as a characteristic signal for identification of the PA radical, which is useful for the thermal decomposition mechanism study. There are five strong IR bands observed for PAN; three strong bands related to the nitroperoxy group, C═O stretching [ν(C═O)], and CH_3 rocking modes. Our calculations show that the nitroperoxy group has three strong infrared bands, which were NO_2 asymmetric stretching [$\nu_a(NO_2)$], NO_2 symmetric stretching [$\nu_s(NO_2)$], and NO_2 scissoring [$\delta(NO_2)$], while experiments[2] reported that three bands are $\nu_a(NO_2)$, $\nu_s(NO_2)$, and the O−N stretching [ν(NO)]. Therefore, the ν(NO) should be assigned as $\delta(NO_2)$. Since the intensity for the NO_2 wagging [γ_w(NO)] is very weak, it is difficult to assign this band experimentally. The other two strong bands, ν(C═O) and CH_3 rocking modes appear at 1909 (1890) and 1192 (1232) cm^{-1}, respectively. The CH_3 rocking mode is coupled with the C−C and the C−O stretching modes. The identification and the gas-phase mechanistic study have been performed with this band, and Gaffney et al.[15] have assigned this band to the C−O stretching mode.

NO_2 and PA radicals are generally less active than PAN in IR spectra. The NO_2 radical shows one strong band at 1727 (2299), which is $\nu_a(NO_2)$. The intensities of $\nu_s(NO_2)$ and δ-(NO_2) modes are weak. The PA radical shows four strong bands at 1929 (1921), 1182 (1216), 1144 (1150), and 751 (780) cm^{-1}, which correspond to ν(C═O), CH_3 rocking, O−O stretching [ν(O−O)], and C−O stretching [ν(C−O)] modes, respectively. The ν(C═O) band for PAN appears at 1909 (1890) cm^{-1}, which is shifted by about 20 cm^{-1} from the PA radical with almost the same intensity. Two bands at 1143 (1150) and 751 (780) cm^{-1} for the PA radical appear at quite different wavenumbers, 977 (937) and 841 (853) cm^{-1}, for PAN, as shown in Figure 2. PAN and PA showed strong IR bands for ν(O−O), which can also be observed in experiments. Furthermore, NO_3, MA, and CH_3CO_2 have no O−O [ν(O−O)] stretching mode. Thus, the vibrational frequencies and the IR intensities of the O−O [ν-(O−O)] stretching mode are useful in identifying the reaction mechanisms.

4. Conclusion

We have studied PAN using B3LYP, MP2, and CCSD(T) methods and compared the predicted results with the experimental data available. The *s-cis*-PAN compound was found to be the global minimum. The predicted enthalpy and entropy changes for the thermal decomposition of PAN are 25.8 kcal/mol and 42.3 cal/(mol·K), respectively, which are in good agreement with the experimental values. The experimentally observed IR band at about 790 cm^{-1} for PAN should be assigned as the NO_2 scissoring [$\delta(NO_2)$] mode. A characteristic IR band of PAN appears at 1232 cm^{-1}, which is a CH_3 rocking mode coupled with CO and OO stretches. The corresponding band of the PA radical appears at 1216 cm^{-1}, about 10 cm^{-1} lower than that of PAN. Thus, determining the concentrations of PAN based on only this band would not be so reliable. We find that the PA radical has a strong IR band at 1150 cm^{-1} due to the O−O stretch mode, while PAN molecule has the corresponding band at 977 cm^{-1}. Since PAN and the PA radical do not have other IR bands at this region, this characteristic band could be used for identification and measurement of the PA radical and for study of the thermal decomposition mechanism of PAN.

Acknowledgment. This research was supported by the Korea Research Foundation (1996-011-D0027).

References and Notes

(1) Roberts, J. M. In *Composition, Chemistry, and Climate of the Atmosphere*; Singh, H. B., Ed.; Van Nostrand Reinhold: New York, 1995.
(2) Roberts, J. M. *Atmos. Environ.* **1990**, *24A*, 243.
(3) Stephenes, E. R.; Hanst, P. L.; Doer, R. C.; Scott. W. E. *Ind. Eng. Chem.* **1956**, *48*, 1498.
(4) (a) Gaffney, J. S.; Marley, N. A.; Prestbo, E. W. *Environ. Sci. Technol*. **1993**, *27*, 1905. (b) Gaffney, J. S.; Marley, N. A.; Prestbo, E. W. In *The Handbook of Environmental Chemistry*; Hutzinger, O., Ed.; Springer-Verlag: Berlin, 1989; Vol. 4, Part B, pp 1−38.
(5) (a) Singh, H. B.; Salas, L. J.; Viezee, W. *Nature* **1986**, *321*, 588. (b) Singh, H. B. *Environ. Sci. Technol*. **1987**, *21*, 320. (c) Singh, H. B.; Salas, L. J. *Nature* **1983**, *302*, 326.
(6) (a) Louw, R.; Van Ham, J.; Nieboer, H. J. *Air Pollut. Control Assoc.* **1973**, *23*, 716. (b) Cox, R. A.; Derwent, R. G.; Holt, P. M.; Kerr, J. A. *J. Chem. Soc., Faraday Trans. 1* **1976**, *72*, 2061.
(7) Miller, C. E.; Lynton, J. I.; Keevil, D. M.; Francisco, J. S. *J. Phys. Chem. A*, in press.
(8) Cox, R. A.; Roffey, M. J. *Environ. Sci. Technol.* **1977**, *11*, 900.

(9) Roberts, J. M.; Bertman, S. B. *Int. J. Chem. Kinet.* **1992**, *24*, 297−307.
(10) Orlando, J. J.; Tyndall, G. S.; Calvert, J. G. *Atmos. Environ.* **1992**, *26A*, 3111−3118.
(11) Bridier, I.; Caralp, F.; Loirat, H.; Lesclaux, R.; Veyret, B.; Becker, K. H.; Reimer, A.; Zabel, F. *J. Phys. Chem.* **1991**, *95*, 3594.
(12) Tauzon, E. C.; Carter, W. P. L.; Atkinson, R. *J. Phys. Chem.* **1991**, *95*, 2434.
(13) Senum, G. I.; Fajer, R.; Gaffney, J. S. *J. Phys. Chem.* **1986**, *90*, 150−156.
(14) Hanst, P. L.; Wong, N. W.; Bragin, J. *Atmos. Environ.* **1982**, *16*, 969.
(15) Gaffney, J. S.; Fajer, R.; Senum, G. I. *Atmos. Environ.* **1984**, *18*, 215.
(16) Niki, H.; Marker, P. D.; Savage, C. M.; Breitenbach, L. P. *Int. J. Chem. Kinet.* **1985**, *17*, 525−534.
(17) Tsalkani, N.; Toupance, G. *Atmos. Environ.* **1989**, *23*, 1849.
(18) (a) Baik, J.; Kim, J.; Majumdar, D.; Kim, K. S. *J. Chem. Phys*. **1999**, *110*, 9116. (b) Lee, H. M.; Kim, J.; Lee, S.; Mhin, B. J.; Kim, K. S. *J. Chem. Phys*. **1999**, *111*, 3995. (c) Kim, J.; Lee, S.; Cho, S. J.; Mhin, B. J.; Kim, K. S. *J. Chem. Phys*. **1995**, *102*, 839.
(19) Hendry, D. G.; Richard, R. A. *J. Am. Chem. Soc.* **1977**, *99*, 3198.
(20) Jursic, B. S. *THEOCHEM* **1996**, *370*, 65.
(21) Frisch, M. J.; Trucks, G. W.; Schlegel, H. B.; Gill, P. M. W.; Johnson, B. G.; Robb, M. A.; Cheeseman, J. R.; Keith, T. A.; Petersson, G. A.; Montgomery, J. A.; Raghavachari, K.; Al-Laham, M. A.; Zakrzewski, V. G.; Ortiz, J. V.; Forseman, J. B.; Cioslowski, J.; Stefanov, B. B.; Nanayakkara, A.; Challacombe, M.; Peng, C. Y.; Ayala, P. Y.; Chen, W.; Wong, M. W.; Andres, J. L.; Replogle, E. S.; Gomperts, R.; Martin, R. L.; Fox, D. J.; Binkely, J. S.; Defrees, D. J.; Baker, J.; Stewart, J. P.; Head-Gordon, M.; Gonzalez, C.; Pople, J. A. *Gaussian 94*; Gaussian, Inc.: Pittsburgh, PA, 1995.
(22) McQuarrie, D. A. *Statistical Mechanics*; Harper & Row: New York, 1973.
(23) Scott, A. P.; Radom, L. *J. Phys. Chem*. **1996**, *100*, 16502.
(24) (a) Lee, J. Y.; Hahn, O.; Lee, S. J.; Choi, H. S.; Shim, H.; Mhin, B. J.; Kim, K. S. *J. Phys. Chem*. **1995**, *99*, 1913. (b) Lee, J. Y.; Hahn, O.; Lee, S. J.; Choi, H. S.; Lee M. S.; Mhin, B. J.; Kim, K. S. *J. Phys. Chem*. **1995**, *99*, 2262.
(25) Rauhut, G.; Pulay, R. *J. Phys. Chem*. **1995**, *99*, 3093.
(26) Pulay, P.; Fogarasi, G.; Pang, P.; Boggs, J. E. *J. Am. Chem. Soc*. **1979**, *101*, 2550.
(27) Houk, K. N.; Lin, Y.-T.; Evansek, J. D. *Angew. Chem., Int. Ed. Engl*. **1992**, *31*, 682.